CANCER

Unexpected contribution of lymphatic vessels to promotion of distant metastatic tumor spread

Qiaoli Ma[1], Lothar C. Dieterich[1], Kristian Ikenberg[1,2], Samia B. Bachmann[1], Johanna Mangana[3], Steven T. Proulx[1], Valerie C. Amann[3], Mitchell P. Levesque[3], Reinhard Dummer[3], Peter Baluk[4], Donald M. McDonald[4], Michael Detmar[1]*

Tumor lymphangiogenesis is accompanied by a higher incidence of sentinel lymph node metastasis and shorter overall survival in several types of cancer. We asked whether tumor lymphangiogenesis might also occur in distant organs with established metastases and whether it might promote further metastatic spread of those metastases to other organs. Using mouse metastasis models, we found that lymphangiogenesis occurred in distant lung metastases and that some metastatic tumor cells were located in lymphatic vessels and draining lymph nodes. In metastasis-bearing lungs of melanoma patients, a higher lymphatic density within and around metastases and lymphatic invasion correlated with poor outcome. Using a transgenic mouse model with inducible expression of vascular endothelial growth factor C (VEGF-C) in the lung, we found greater growth of lung metastases, with more abundant dissemination to other organs. Our findings reveal unexpected contributions of lymphatics in distant organs to the promotion of growth of metastases and their further spread to other organs, with potential clinical implications for adjuvant therapies in patients with metastatic cancer.

INTRODUCTION

Tumor lymphangiogenesis plays an important role in cancer progression to sentinel lymph nodes (*1*, *2*), and expression of the lymphangiogenic factor vascular endothelial growth factor C (VEGF-C), higher lymphatic vessel (LV) density, and the presence of tumor cells within LVs, termed lymphatic invasion, are associated with poor prognosis in many different types of cancer (*1*–*3*). Lymphangiogenesis also occurs in the sentinel lymph node, sometimes even before the arrival of metastatic tumor cells, stimulated by lymphangiogenic factors drained from the primary tumor (*4*–*6*). Besides providing a route for metastatic tumor cells, LVs might also contribute to tumor progression by providing a "niche" for cancer stem-like cells (*7*), which might facilitate the formation of "in-transit" melanoma metastases. Lymphatic endothelial cells (LECs) in primary tumors and tumor-draining lymph nodes might also present tumor antigens and suppress $CD8^+$ T cell activation (*8*), thereby protecting metastatic cells from antitumor immune reactions.

Sentinel lymph node metastasis represents an important prognostic indicator for systemic spread and for reduced survival in many cancer types, including melanoma and breast cancer. While recent studies indicated that cancer cells colonizing the sentinel lymph node might contribute to the seeding of visceral organ metastasis (*9*–*11*), surgical resection of regional lymph nodes did not improve the overall survival rate compared to radiation and systemic therapy without surgical resection of regional lymph nodes in breast cancer and melanoma patients (*12*–*14*). Thus, it currently remains a conundrum how tumor and lymph node lymphangiogenesis might contribute to reduced patient survival. Recently, genome sequencing studies of multiple organ and lymph node metastases of prostate cancer patients have provided evidence that organ-to-organ metastasis might be commonly occurring in cancer (*10*, *11*). This led us to hypothesize that lymphangiogenesis occurring within metastases might enable those metastases to seed additional metastases in other organs.

Here, we used two metastasis mouse models, a B16F10 melanoma model and an orthotopic 4T1 breast cancer model, to investigate whether lymphangiogenesis occurs at distant sites and might be correlated with further metastases. We also used a genetic mouse model to increase LV density in the lungs and investigated the growth of experimental melanoma- and breast cancer–derived lung metastases and spread from the lungs to other organs. Furthermore, we retrospectively analyzed 266 melanoma patients with lung metastases and quantified LVs in resected lung tissue with metastases in a subgroup of 26 patients. Our findings reveal an unanticipated role of LVs in the promotion of the growth of metastases established in distant organs and their further metastatic spread to other organs, with potential clinical implications for adjuvant therapies in patients with metastatic cancer.

RESULTS

Lymphangiogenesis occurs in metastasis-bearing lungs

Tumor-associated lymphangiogenesis is commonly seen in primary tumors and sentinel lymph nodes and is associated with poor prognosis (*1*, *2*). We wondered whether lymphangiogenesis might also occur in distant organ metastases. Therefore, we orthotopically implanted spontaneously metastasizing 4T1 breast cancer cells into the fourth mammary fat pad and removed the primary tumors 21 days later. A further 21 days after primary tumor removal, when most mice had developed overt lung metastasis, we compared the lymphatic density in the control lungs and non-nodule covered area in the lungs of 4T1-injected mice. Thy1 (*15*–*17*) was used to identify pulmonary LVs, and cytokeratin was used to identify 4T1 cells (Fig. 1A and fig. S1). The lung area occupied by LVs was significantly larger in 4T1-injected mice compared with naïve lungs (4.86 ± 2.00%

[1]Institute of Pharmaceutical Sciences, Swiss Federal Institute of Technology, ETH Zurich, Zurich, Switzerland. [2]Department of Pathology and Molecular Pathology, University Hospital Zurich, Zurich, Switzerland. [3]Department of Dermatology, Skin Cancer Center, University Hospital Zurich, Zurich, Switzerland. [4]UCSF Helen Diller Family Comprehensive Cancer Center, Cardiovascular Research Institute and Department of Anatomy, University of California, San Francisco, San Francisco, CA 94143, USA. *Corresponding author. Email: michael.detmar@pharma.ethz.ch

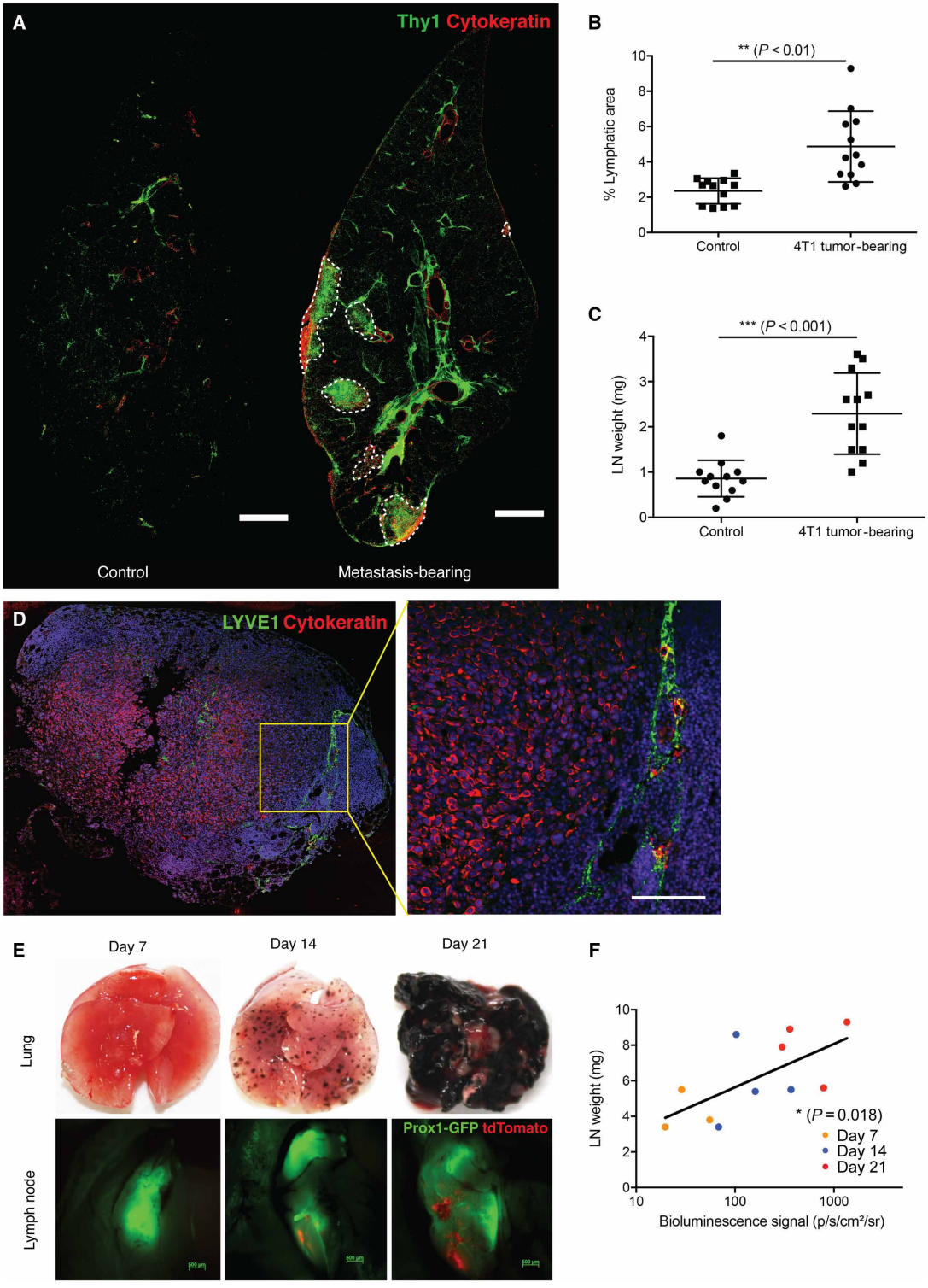

Fig. 1. Lymphangiogenesis in metastasis-bearing lungs. 4T1-luc2 cells (1×10^5) were orthotopically inoculated, and after 21 days, the primary tumors were removed. Twenty-one days after the operation, mice were sacrificed for analysis. (**A**) Representative images of a naïve lung and a metastasis-bearing lung. White dashed line indicates the edge of a metastatic nodule. Scale bars, 500 μm. (**B**) Quantification of Thy1$^+$ area in the lungs of control mice and non-nodule covered lung area of 4T1-injected mice ($n = 12$). (**C**) Quantification of the lung-draining (tracheobronchial) lymph node (LN) weight ($n = 12$). (**D**) Representative images of 4T1 cells metastasized to a tracheobronchial lymph node. Scale bar, 50 μm. (**E** and **F**) Prox1-GFP mice were inoculated with 5×10^5 B16F10-luc2-tdTomato cells intravenously and were sacrificed on days 7, 14, and 21 after injection. (**E**) Representative images of lungs and tracheobronchial lymph nodes. Lymph nodes were imaged in situ using a fluorescence stereomicroscope. Scale bars, 500 μm. (**F**) Correlation between lung metastasis (quantified by bioluminescence signal from B16F10-luc2-tdTomato cells) and lymph node weight ($n = 11$). Nonparametric correlation (Spearman) with nonlinear regression analysis was performed.

versus 2.35 ± 0.73%, $P < 0.01$, Fig. 1B). We next investigated the tracheobronchial lymph nodes of 4T1-injected mice. The weight of lung-draining lymph nodes in these mice was significantly greater than in normal controls (2.29 ± 0.90 mg versus 0.86 ± 0.40 mg, $P < 0.001$, Fig. 1C). Because a weight increase of tumor-draining lymph nodes is not an exact measure for metastatic colonization, we next performed immunofluorescence staining of the lymph nodes for cytokeratin. Tumor cells were detected in about 30% of the lung-draining lymph nodes (Fig. 1D). Comparable results were obtained in an experimental melanoma metastasis model, in which B16F10 melanoma cells expressing luciferase (luc2) and the fluorescent reporter tdTomato were injected into the tail vein. The resulting metastases in the lungs were accompanied by an increased tdTomato fluorescence signal in the draining lymph nodes (Fig. 1E), and there was a significant correlation between the extent of lung metastases (quantified by bioluminescence) and the weight of the lung-draining lymph nodes (Spearman correlation, $P = 0.018$; nonlinear regression, $r^2 = 0.42$; Fig. 1F). Together, these data reveal that, as in the primary tumor, lymphangiogenesis also occurred in metastases. Therefore, we next investigated whether lymphangiogenesis at sites of metastasis might contribute to further tumor spread to other organs and correlate with poor patient outcome.

High lymphatic density and lymphatic invasion in metastasis-bearing lungs correlate with poor prognosis in melanoma patients

To study the prognostic relevance of lymphangiogenesis at sites of metastasis, we conducted a retrospective study of 266 melanoma patients with lung metastasis (fig. S2A). Tumor cells in lung-draining lymph nodes (fig. S2B) were detected in 60.2% of the 266 patients. Surgically resected lung samples were available from 26 of these patients (fig. S2C). LVs stained for podoplanin with the D2-40 antibody were quantified around (Fig. 2A and fig. S3A) and within metastases in the lungs (Fig. 2B and fig. S3, B and C). The area covered by lymphatics (Fig. 2C) and LV density (the number of LVs per square millimeter) (fig. S3D) were significantly greater around lung metastases in patients who also had metastases in lung-draining lymph nodes (3.73 ± 2.09% versus 2.05 ± 1.50%, $P < 0.05$, Fig. 2C; 33.93 ± 19.33 LV/mm^2 versus 18.64 ± 12.49 LV/mm^2, $P < 0.05$, fig. S3D). Similarly, the lymphatic area was greater within metastases in patients who also had metastases in lung-draining lymph nodes (2.09 ± 1.70% versus 1.00 ± 0.47%, $P < 0.05$, Fig. 2D). The LV density showed the same trend without reaching significance (30.94 ± 25.45 LV/mm^2 versus 19.6 ± 14.97 LV/mm^2, $P = 0.22$, fig. S3E). Patients with lymphatic area and lymphatic density values around metastases above the median had a significantly shorter survival time than those with values below the median (14.07 ± 2.16 months versus 38.69 ± 5.44 months, $P = 0.001$, Fig. 2E; 17.02 ± 3.17 months versus 36.47 ± 6.08 months, $P = 0.019$, fig. S3F). Similarly, high values for lymphatic area within metastases correlated with poor prognosis (16.87 ± 2.97 months versus 35.87 ± 6.54 months, $P = 0.045$, Fig. 2F). The difference in LV density was not significant but followed the same trend (21.09 ± 5.62 months versus 33.45 ± 5.73 months, $P = 0.16$, fig. S3G).

In melanoma, lymphatic invasion in the primary tumor is frequently related to sentinel lymph node metastasis and correlates with poor prognosis (*18*, *19*). We next analyzed the incidence of lymphatic invasion (Fig. 2G) at the site of lung metastases. Lymphatic invasion, defined by the presence of tumor cells within D2-40–positive LVs, was seen more frequently in patients with metastases in lung-draining lymph nodes than in those without (12 of 15 versus 2 of 11, $P = 0.0043$, Fig. 2H). Furthermore, patients with lymphatic invasion had a shorter survival time (19.56 ± 2.94 months versus 36.03 ± 7.21 months, $P = 0.085$, Fig. 2I). These data provide the first clinical evidence that lymphatic density within and around metastases and lymphatic invasion correlate with poor prognosis. These findings also raise the possibility that LVs support the growth of metastases and/or facilitate further tumor spread to other organs.

Immune cell infiltration is commonly seen in many types of tumors, and its prognostic value has been reported (*20*, *21*). Immune cells are important players in the tumor microenvironment, actively interacting with other tumor-surrounding components, including tumor-associated LVs. To study the potential correlation between immune cell infiltration and lymphangiogenesis, the degree of immune cell infiltration in the lung sections with melanoma metastases was scored semiquantitatively by a board-certified pathologist (fig. S4A), and the LV density (percentage of tissue area covered by LVs) was analyzed for each sample. There was a clear trend for an increased LV density in the group of patients with a higher degree of immune cell infiltration; however, no statistical significance was reached [$P = 0.052$, one-way analysis of variance (ANOVA); fig. S4B]. We also compared the degree of immune cell infiltration between patients with and without lung-draining lymph node metastasis (fig. S4C). Statistical analysis (χ^2 test) did not detect a significant difference ($P = 0.18$); however, the patients with the highest degree of immune cell infiltration all had metastases in the lung-draining lymph node.

Inducible transgenic overexpression of VEGF-C in the lungs of mice results in increased LV density

To study the function of LVs at sites of distant metastasis in more detail, we used an inducible, Clara cell promoter-driven transgenic mouse model to overexpress VEGF-C in the airway (CCSP-rtTA × tet-O–VEGF-C; CCSP × VEGFC) (*22*, *23*).

In pilot studies, we induced VEGF-C overexpression in 8-week-old mice by applying different concentrations of doxycycline for 2 weeks to identify a dose that reliably induces LV growth without causing chylothorax. On the basis of these studies, a doxycycline concentration of 1 mg/ml was chosen for mice in the C57BL/6 background and 2 mg/ml for mice in the BALB/c background. After 2 weeks of doxycycline treatment of C57BL/6 mice, VEGF-C mRNA expression in the lung was increased more than 25-fold compared to control wild-type × tet-O–VEGF-C (WT × VEGFC) mice ($P < 0.001$, Fig. 3A). The VEGF-C protein concentration in the lung increased to 141.7 ± 22.24 pg/mg tissue compared to 80.67 ± 23.5 pg/mg tissue in control mice ($P = 0.001$, Fig. 3B). Accordingly, the area of VEGFR3$^+$ (VEGF receptor 3–positive) lymphatics was almost threefold greater than in controls (8.66 ± 1.95% versus 2.98 ± 0.25%, $P < 0.01$; Fig. 3, C and D). Lung lymphatics around bronchi and pulmonary veins were more abundant but otherwise appeared normal. Lymphatics were also more abundant beneath the visceral pleura of CCSP × VEGFC mice but were sparse or absent in controls (Fig. 3E). The morphology (Fig. 3F) and density (Fig. 3G) of blood vessels were not affected by VEGF-C overexpression.

Metastasis in lungs and other organs is greater in mice with VEGF-C overexpression in the lungs

To determine whether lymphatic growth induced by VEGF-C overexpression in the lung increased metastases, 5×10^5 B16F10-luc2-tdTomato tumor cells were injected via the tail vein of doxycycline-treated

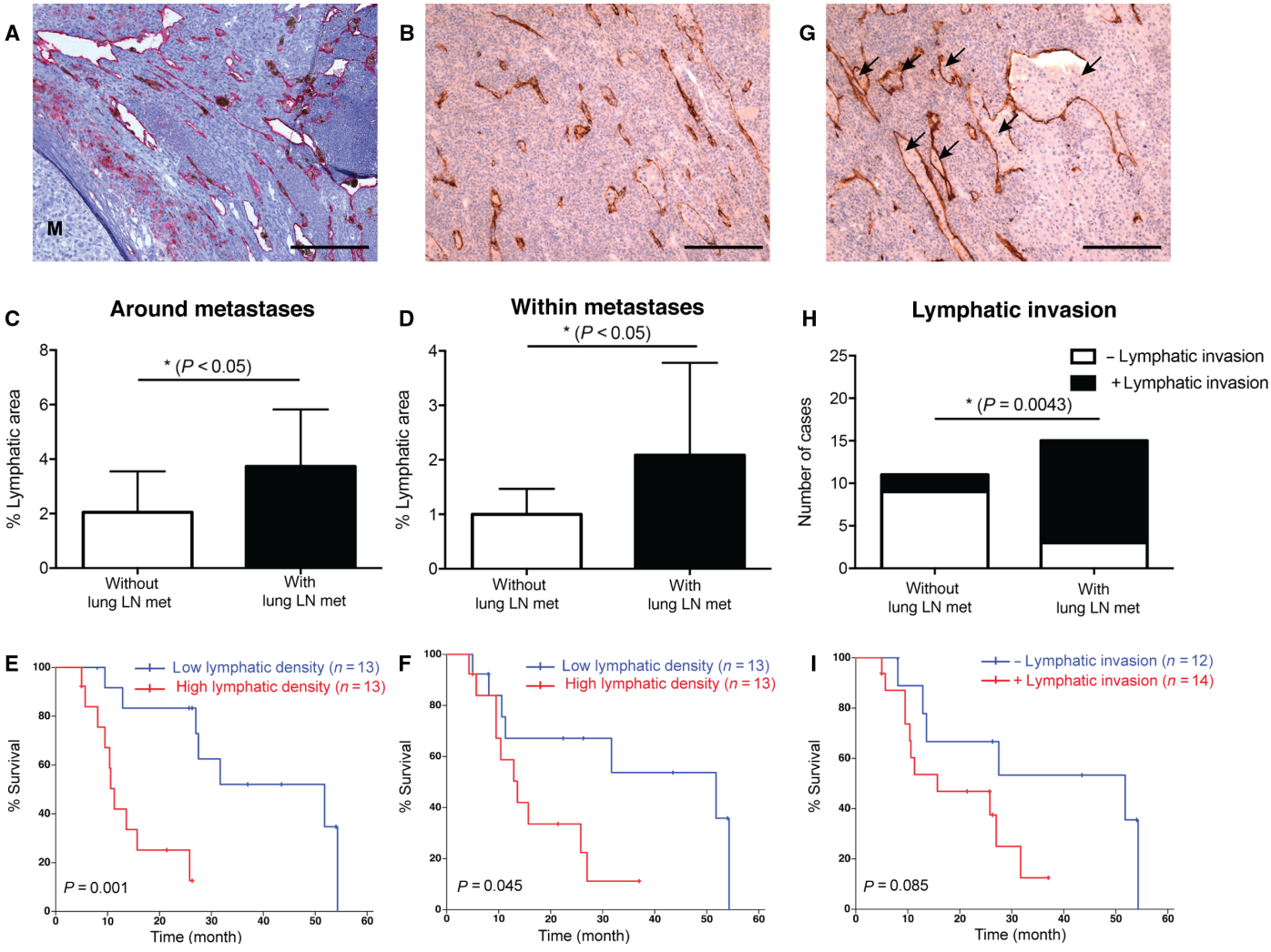

Fig. 2. High lymphatic density and lymphatic invasion in metastasis-bearing lungs correlate with poor prognosis of melanoma patients. (**A** and **B**) Representative images of lymphatic hotspots (stained for podoplanin) around (A) and within (B) metastases in the lung. The metastasis area is labeled with "M." Scale bars, 200 μm. (**C** and **D**) Quantification of the percentage of lymphatic area around (C) and within (D) metastases in the lungs of patients without (white bars; $n = 11$) and with (black bars; $n = 15$) lung-draining lymph node metastasis. (**E** and **F**) Kaplan-Meier survival analysis of patients with low lymphatic area (below median; $n = 13$) and high lymphatic area (above median; $n = 13$) around (E) and within (F) metastases in the lungs. (**G**) Representative image of lymphatic invasion in a melanoma lung metastasis. Scale bar, 200 μm. Tissues shown in (B) and (G) were located within a larger metastatic region containing cancer cells (see fig. S3C). (**H**) Quantification of incidence of lymphatic invasion in patients without ($n = 11$) and with ($n = 15$) lung-draining lymph node metastasis. Fisher's exact test was performed. (**I**) Kaplan-Meier survival analysis of patients with (+; $n = 14$) and without (–; $n = 12$) lymphatic invasion. The time axes indicate the time from detection of lung metastases until death. Log-rank (Mantel-Cox) test was performed.

CCSP × VEGFC mice, and 14 days later, the metastatic load in the lungs was evaluated by measuring the tdTomato [red fluorescent protein (RFP)]–positive area (Fig. 4A). WT × VEGFC mice were used as controls. This analysis revealed greater metastatic growth (20.69 ± 8.54% versus 14.42 ± 3.82%, $P < 0.05$; Fig. 4, B and C) in the lungs of CCSP × VEGFC mice. Measurements of tdTomato-positive cells at 24 hours after intravenous injection indicated that the difference did not reflect greater initial tumor cell homing to the lungs of CCSP × VEGFC mice (Fig. 4D). Fourteen days after tumor cell injection, the number of metastatic nodules in the lung was also comparable (fig. S5A). In VEGF-C–overexpressing mice, there were slightly, but not significantly, more large- and medium-sized nodules compared with control mice (fig. S5B). Most metastatic nodules were near bronchi, whereas in control mice, metastatic nodules were scattered throughout the lungs, including near the pleural surface. The incidence of lymphatic invasion was greater in VEGF-C–overexpressing lungs (6 of 10 versus 0 of 10, $P = 0.0034$, Fig. 4E), as was the weight of the lung-draining lymph nodes (3.59 ± 1.34 mg versus 2.45 ± 0.67 mg, $P < 0.05$, Fig. 4F). Metastases were also more numerous in other organs of mice with VEGF-C overexpression in the lungs. In the CCSP × VEGFC group, 10 of 15 mice had metastases in other organs beside the lungs, while in the control group, only 3 of 15 mice also had metastases in other organs, indicating that CCSP × VEGFC mice are 7.4 times more likely to have metastasis in other organs compared to the control group (odds ratio, 7.4; $P = 0.025$, Fisher's exact test). Furthermore, we quantified the number of organs with metastasis including the liver, intestine, brain, and kidney in each mouse (Fig. 4G) and performed a quasi-Poisson regression analysis to estimate

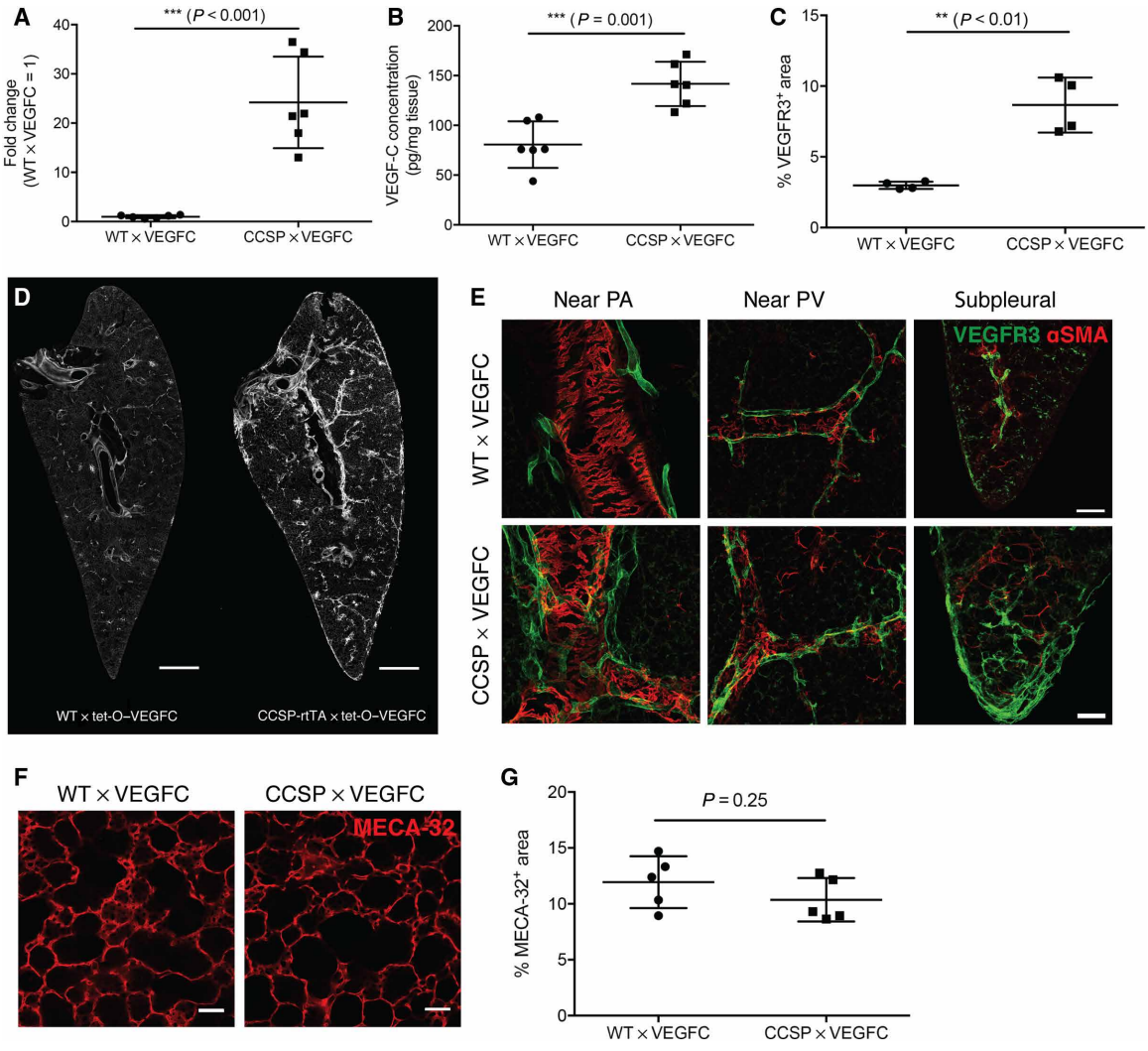

Fig. 3. Characterization of CCSP-rtTA × tet-O–VEGF-C mice after doxycycline treatment for 2 weeks. (**A**) VEGF-C mRNA expression in the lung (normalized to RPLP0). The average expression level in WT × tet-O–VEGF-C mice was set to 1 ($n = 6$). (**B**) VEGF-C protein levels in the lung detected by enzyme-linked immunosorbent assay (ELISA) ($n = 6$). (**C**) Quantification of the VEGFR3$^+$ LV area ($n = 4$). (**D**) Representative images of VEGFR3 staining in the lung. Scale bars, 1 mm. (**E**) Representative high-magnification images of different regions in the lung stained for VEGFR3. Scale bars, 200 μm. PA, pulmonary artery; PV, pulmonary vein. (**F**) Representative images of MECA-32 staining in the lung. Scale bars, 50 μm. (**G**) Quantification of MECA-32$^+$ blood vessel area in the lung ($n = 5$).

the expected number of affected organs per animal. CCSP × VEGFC mice had 3.6 times more organs affected than control mice (1.2 organs per mouse in CCSP × VEGFC mice versus 0.33 in control mice; $P = 0.025$), suggesting a greater spread of melanoma cells through lung lymphatics.

VEGF-C expressed in the lung could reach the circulation and promote lymphatic growth and metastasis in other organs. We addressed this issue by measuring VEGF-C mRNA expression, protein levels, and LV density and morphology in the liver and intestine, two common sites of metastasis. After 2 weeks of VEGF-C induction, VEGF-C mRNA expression (1.19 ± 0.66 versus 1.00 ± 0.27, $P = 0.52$, fig. S6A) and protein levels were comparable in the liver (3.31 ± 0.59 μg/mg tissue versus 3.37 ± 0.84 μg/mg tissue, $P = 0.89$, fig. S6B) and intestine (mRNA: 1.04 ± 0.25 versus 1.00 ± 0.12, $P = 0.75$, fig. S6A; protein: 47.99 ± 17.94 pg/mg tissue versus 54.79 ± 13.42 pg/mg tissue, $P = 0.47$, fig. S6B). VEGF-C protein levels were slightly higher in the serum (24.85 ± 12.69 pg/ml versus 13.52 ± 6.00 pg/ml, $P = 0.14$, fig. S6B). The density and morphology of LVs in the intestine and liver were comparable in CCSP × VEGFC and control mice (fig. S6, C and E). The width of intestinal lacteals was similar in CCSP × VEGFC and control mice (fig. S6D).

As mechanisms of lung colonization after tail vein injection of B16F10 cells are likely to differ from spontaneously forming lung metastases, we next investigated the effects of increased lung lymphatic density in the 4T1 orthotopic breast cancer model. CCSP × VEGFC mice, bred into the BALB/c background, showed a similar extent of lung lymphangiogenesis as CCSP × VEGFC mice on the C57BL/6 background when a higher dose (2 mg/ml) of doxycycline was used (fig. S7). As before, 1×10^5 4T1-luc2 cells were orthotopically injected and primary tumors were removed after 21 days. Four days after the surgery, VEGF-C overexpression was induced in the lung. On days 7, 14, and 21, in vivo IVIS imaging was performed to detect the metastases, and 21 days after the surgery, lungs and other organs were resected after euthanization and were quantified ex vivo

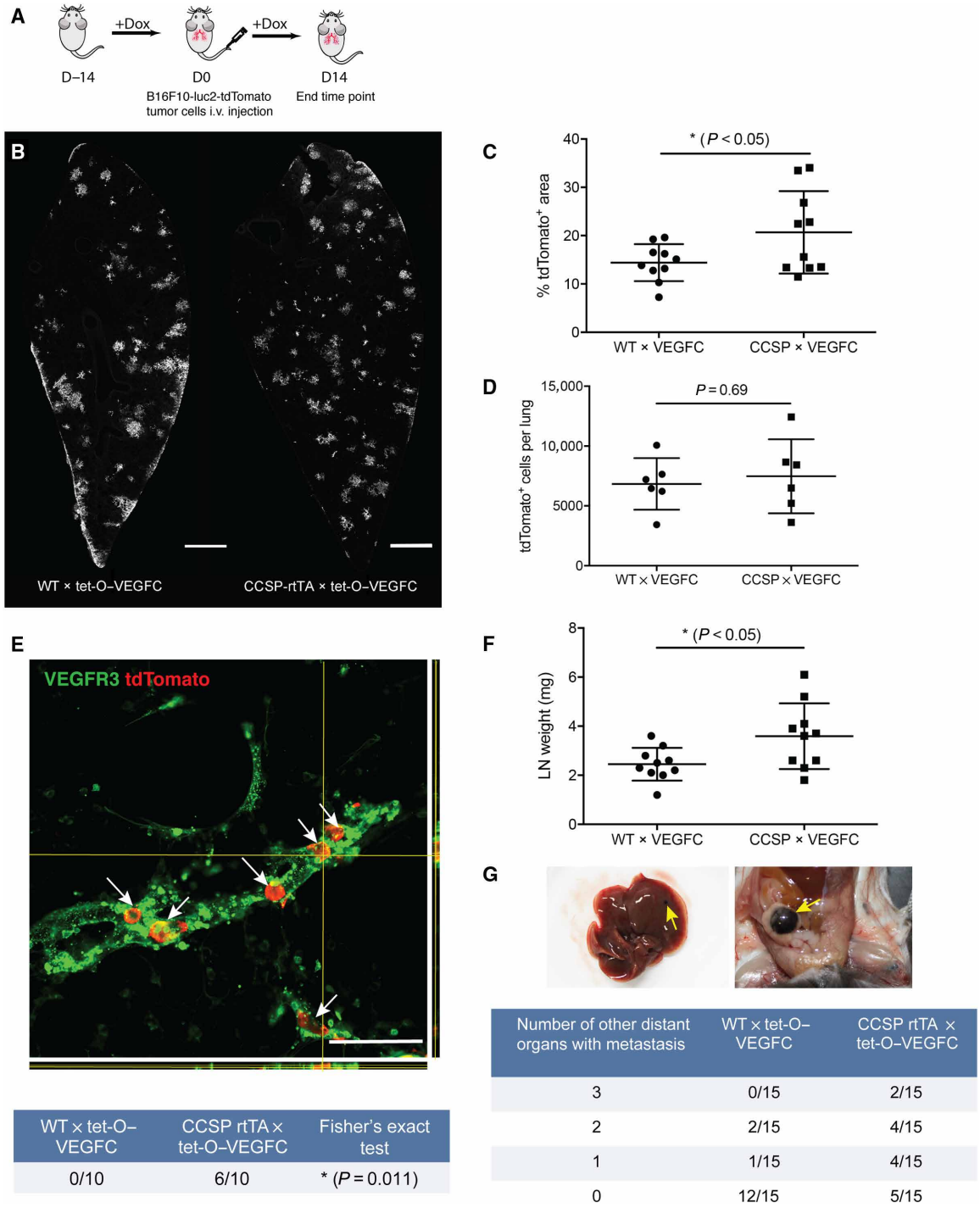

WT × tet-O–VEGFC	CCSP rtTA × tet-O–VEGFC	Fisher's exact test
0/10	6/10	* ($P = 0.011$)

Number of other distant organs with metastasis	WT × tet-O–VEGFC	CCSP rtTA × tet-O–VEGFC
3	0/15	2/15
2	2/15	4/15
1	1/15	4/15
0	12/15	5/15

Fig. 4. Increased metastasis in CCSP-rtTA × tet-O–VEGF-C mice after tail vein injection of B16F10 melanoma cells. (**A**) Schematic of the B16F10 tumor study. Dox, doxycycline; i.v., intravenous. (**B**) Representative images of lung sections with metastatic nodules 14 days after tumor cell injection (indicated by staining for RFP from B16F10-luc2-tdTomato cells). Scale bars, 1 mm. (**C**) Quantification of tdTomato$^+$ area in the lung 14 days after tumor cell injection ($n = 10$). (**D**) Quantification of tdTomato$^+$ cells per lung 24 hours after intravenous injection of 1×10^6 B16F10-luc2-tdTomato cells. (**E**) Representative images of lymphatic invasion (white arrows) with orthogonal projection. Scale bars, 100 μm. Fisher's exact test was performed. (**F**) Quantification of the lung-draining lymph node weight ($n = 10$). (**G**) Number of mice with different numbers of distant organs with metastasis (zero, one, two, or three organs affected) and example images of metastases (yellow arrows) in the liver and intestine. Data were pooled from two rounds of studies.

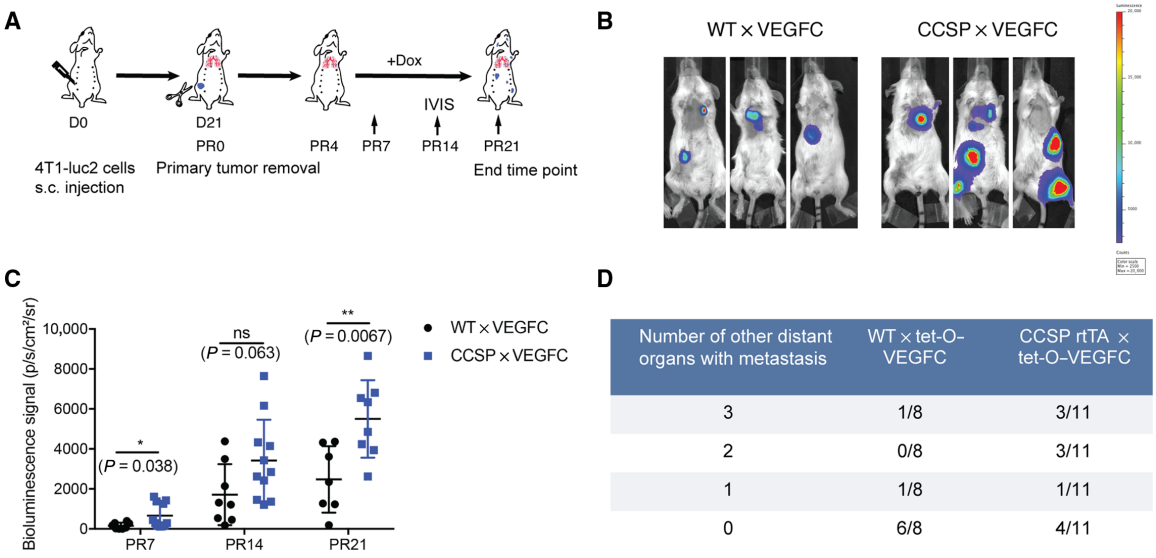

D

Number of other distant organs with metastasis	WT × tet-O-VEGFC	CCSP rtTA × tet-O–VEGFC
3	1/8	3/11
2	0/8	3/11
1	1/8	1/11
0	6/8	4/11

Fig. 5. Increased metastasis in CCSP-rtTA × tet-O–VEGF-C mice in the 4T1 spontaneous breast cancer metastasis model. (**A**) Schematic of the 4T1 tumor study. PR, postremoval; s.c., subcutaneous. (**B**) Representative in vivo bioluminescence images of metastases on day 21 after primary tumor removal. (**C**) Quantification of bioluminescence signal over the whole body on days PR7, PR14, and PR21 by IVIS imaging. For data from days PR7 and PR14, WT × VEGFC, $n = 8$, and CCSP × VEGFC, $n = 11$. Four mice reached the euthanization criteria before the end time point; thus, for data from day PR 21, WT × VEGFC, $n = 7$, and CCSP × VEGFC, $n = 8$. ns, not significant. (**D**) Number of mice with different numbers of distant organs with metastasis (zero, one, two, or three organs affected). Data were pooled from three rounds of studies. Only mice with detectable metastases (by ex vivo IVIS imaging) in the lungs were quantified.

(Fig. 5A). The primary tumor growth (fig. S8, A and B) and the incidence of lung metastasis (fig. S8C) at the time of primary tumor removal were comparable. Twenty-one days after primary tumor removal (17 days after induction of VEGF-C), overt lung metastasis was detectable in 8 of 16 mice in the control group. Of these, one mouse had to be euthanized before the predefined study end point. In mice with VEGF-C overexpression in the lung, 11 of 16 mice showed detectable lung metastases, of which 3 mice reached the euthanization criteria before the end point. Because of the high variability of spontaneously formed metastasis, we did not observe a significant difference in nodule number and size (fig. S9). Strikingly, the metastatic load over the whole body, monitored by bioluminescence imaging, was much greater in CCSP × VEGFC mice (Fig. 5, B and C). CCSP × VEGFC mice were 4.8 times more likely to have metastasis in other organs compared to the control group (7 of 11 mice in the CCSP × VEGFC group versus 2 of 8 mice in the control group; odds ratio, 4.8; $P = 0.17$, Fisher's exact test). Quasi-Poisson regression analysis estimated that 2.9 times more organs were affected in CCSP × VEGFC mice than in control mice (1.45 organs per mouse in CCSP × VEGFC mice versus 0.5 in control mice; $P = 0.13$; Fig. 5D and fig. S10). Together, these data further support the concept that metastasis-associated lymphatics might facilitate the spread of lung metastases to other organs.

DISCUSSION

In many cancer types, including melanoma and breast cancer, VEGF-C expression, tumor-associated lymphangiogenesis, and lymphatic invasion within the primary tumor correlate with poor patient outcome and have been suggested as prognostic markers (*1*–*3*). In this study, we demonstrate that lymphangiogenesis is also induced at sites of metastasis. Lymphangiogenesis and the presence of lymphatic invasion within and around metastases in the lung correlated with poor outcome in a cohort of melanoma patients. Lymphatic density and invasion in metastases could serve as prognostic factors for late-stage melanoma patients with visceral organ metastasis or for patients with melanoma metastases but without apparent primary tumor.

Increased LV density at metastatic sites, especially in combination with lymphatic invasion, could facilitate further lymphatic spread of metastatic cells from established metastases at the distant sites. In our cohort of melanoma patients, lymphangiogenesis and lymphatic invasion in and around metastases in the lungs correlated with the presence of metastases in hilar lymph nodes. Similarly, in experimental tumor models, greater lymphatic area in metastasis-bearing lungs and greater weight of the tracheobronchial lymph node were associated with the presence of further distant metastasis. Using a transgenic mouse model with inducible VEGF-C expression and lymphangiogenesis in the lung, we found greater growth of experimental melanoma metastases in the lungs and more metastases in other organs in both the melanoma and the breast cancer model. The further distant metastatic spread from lung metastases seems to be mediated by the increased access to LVs and not just by enhanced growth of lung metastases, because there was no major difference in the distant metastasis rate in CCSP × VEGFC mice with high versus low metastatic load in the lung. Accordingly, the incidence of lymphatic invasion and the weight of draining lymph nodes were both greater in lungs with expanded lymphatics after VEGF-C overexpression. These findings are in agreement with a previous study in nude mice, where VEGF-C overexpression in the tumor cells promoted intralymphatic spread of lung metastases (*24*). It will be of great interest to investigate, in future studies, whether LVs might also promote the growth and/or further spread of metastases in other organs than the lungs.

The contribution of lymph node metastasis to metastases in other organs has remained unclear, although the detection of sentinel lymph node metastasis is associated with reduced survival in many tumor

types (*1*, *2*). However, surgical resection of regional lymph nodes did not improve the overall survival rate compared to radiation and systemic therapy without surgical resection of regional lymph nodes in melanoma and breast cancer patients (*12*–*14*). Our results provide a possible explanation for this apparent discrepancy; the presence of sentinel lymph node metastasis might reflect the potential of disseminated tumor cells to induce lymphangiogenesis at distant sites, which might promote further metastatic progression to other distant organs. In line with this hypothesis, chemokines produced by LECs have been reported to attract CXCR4-expressing melanoma stem-like cells, resulting in a "lymphovascular niche," whereas CCR7, the receptor for the lymphatic chemokine CCL21, promoted stemness in breast cancer (*7*, *25*).

Our finding that the density of blood vessels in the lung was unaffected despite the large expansion of the lymphatic network by VEGF-C overexpression is in line with previous studies in which lymphangiogenesis, but not angiogenesis, was found in transgenic mice overexpressing VEGF-C (*26*, *27*). Although the mature form of VEGF-C can bind to the major angiogenesis receptor VEGFR2 on blood vascular endothelium, its affinity for VEGFR3 is much higher (*28*). Together with our finding that extravasation of tail vein–injected tumor cells from the bloodstream to the lung parenchyma was not increased in VEGF-C–overexpressing lungs, an influence of blood vessel activation on metastatic growth and secondary organ-to-organ metastasis via blood vessels seems unlikely. A direct mitogenic effect of VEGF-C on metastatic tumor cells also seems unlikely, because we could not detect VEGFR3 expression on B16F10 and 4T1 cells by quantitative polymerase chain reaction (qPCR) and immunofluorescence staining, and because there was no increase in the proliferation rate of B16F10 cells upon VEGF-C treatment in vitro.

In conclusion, our study shows that, besides promoting the spread of tumor cells from primary tumors to tumor-draining lymph nodes, lymphangiogenesis can also facilitate further metastasis by promoting the growth of metastases in distant organs and their further dissemination to other distant organs. Anti-lymphangiogenic agents could have beneficial effects in patients with metastatic cancers.

MATERIALS AND METHODS

Mice

C57BL/6J and BALB/c WT mice were obtained from Janvier. CCSP-rtTA × tet-O–VEGF-C mice (*22*, *23*) were backcrossed into the C57BL/6 and BALB/c backgrounds. Prox1-GFP mice were provided by Y.-K. Hong, University of Southern California (*29*). All mice were housed under specific pathogen–free conditions. The overexpression of VEGF-C in CCSP-rtTA × tet-O–VEGF-C mice was induced by administration of doxycycline (1 mg/ml, C57BL/6 mice; 2 mg/ml, BALB/c mice) in drinking water (containing 5% sucrose) for 2 weeks, starting at 8 weeks of age.

Tumor studies

For the B16F10 metastasis model, 5×10^5 B16F10-luc2-tdTomato cells were suspended in 200 μl of phosphate-buffered saline (PBS) and injected into the tail vein. The mice were monitored three times a week for up to 3 weeks. For the 4T1-luc2 spontaneous breast cancer metastasis model, 1×10^5 tumor cells were suspended in 50 μl of PBS and injected into the fourth mammary fat pad of BALB/c mice. The primary tumor growth was monitored every 3 days for 3 weeks until the primary tumors were surgically removed. After the surgery, mice were monitored three times a week for another 3 weeks. The mice were euthanized with an overdose of anesthesia [ketamine (1000 mg/kg), Ketasol, Graeub; medetomidine (3.5 mg/kg), Domitor, Provet], and tissues were collected for analysis. All tumor studies were performed in agreement with the regulations of the local ethical board of Kantonales Veterinäramt Zürich, under license ZH012/15.

Retrospective lung metastasis study

The information on melanoma patients and lung samples was collected at the Department of Dermatology at the University Hospital Zurich. Resected lung samples of patients with melanoma metastasis ($n = 26$) were sectioned at a thickness of 4 μm and stained for podoplanin (clone D2-40, BioLegend). The LV hotspots around and within metastases were imaged on a Zeiss Axioskop 2 MOT Plus microscope with a 20× objective. The LV number and lymphatic area percentages were quantified in a blinded manner from patient information. Five hotspots per sample were analyzed, and the average value was calculated for each sample. The incidence of lymphatic invasion was determined on the basis of the entire sample. The local ethics committee approved the written informed consent for tissue storage including the retrospective analysis with collection of clinical/laboratory/histological information before collection (Kantonale Ethikkommission Zürich, Biobank/Sammlung von Tumorgewebe, KEK-ZH-Nr. 647).

Tissue processing and immunofluorescence staining

For lung staining, the mouse lungs were filled with 2% low-melt agarose (Bio-Rad) through the trachea before dissection, chilled down in ice-cold PBS, and fixed in 4% paraformaldehyde (PFA) for 2 hours. For sectioning, agarose-filled lungs were embedded in 2% low-melt agarose and sectioned by Vibratome (Leica VT1000 S) into 200-μm-thick slices before staining. In the studies to compare the pulmonary lymphatic density in CCSP × VEGFC with WT × VEGFC mice, transverse sections from the part near the left bronchial branch of the left lobe were used for staining. In the study to compare the pulmonary lymphatic density in the lungs of control and 4T1-injected mice, transverse sections were made at the position of the detected nodules and corresponding positions in the control lungs. For the lungs without visible nodules on the surface, sections from the part near the left bronchus of the left lobe were used. For lacteal staining, approximately 1 cm of small intestine after the pancreatic curve was dissected, and the tube was cut longitudinally and pinned down (inside up) in silicone gel–coated six-well plates and fixed in 4% PFA for 2 hours at 4°C before staining. For liver staining, the right lobe of the mouse liver was dissected and fixed in 4% PFA for 2 hours at 4°C. Longitudinal sections (200 μm) were cut by Vibratome (Leica VT1000 S) before staining. Lymph nodes and other organs were dissected, embedded in OCT (optimal cutting temperature) compound, snap-frozen, and stored at −80°C until preparation of cryosections (7 μm).

For immunofluorescence stainings, sections were fixed with 4% PFA for 20 min, rinsed with PBS, and blocked in PBS with 0.2% bovine serum albumin, 5% donkey serum, and 0.3% Triton X-100 (blocking solution). Primary antibodies suspended in the blocking solution were incubated at room temperature for 2 hours or at 4°C overnight, followed by extensive washing and incubation with secondary antibodies. The antibodies used were Thy1.2 (rat, eBioscience), cytokeratin (wide spectrum, rabbit, Dako), LYVE-1 (rabbit, AngioBio), αSMA-Cy3 (mouse, Sigma-Aldrich), VEGFR3 (goat, R&D Systems), MECA-32 (rat, BD), RFP (rabbit, Rockland), podoplanin (goat, R&D Systems), and CD31 (rat, BD Pharmingen).

Image analysis

Images were taken on a Zeiss Axioskop 2 MOT Plus microscope with 10× or 20× objective, or a Zeiss LSM 880 upright confocal microscope with 20× objective. Image analysis was performed using ImageJ (National Institutes of Health). For the quantification of the Thy1$^+$ lymphatic area, structures smaller than 150 μm^2 were excluded.

Bioluminescence and stereomicroscope imaging

Bioluminescence imaging was performed with an IVIS Spectrum system (PerkinElmer). Fifteen minutes after intraperitoneal injection of D-luciferin (10 μl/g; 15 mg/ml in PBS; PerkinElmer), mice were anesthetized by inhalation of 2% isoflurane in O_2, placed on the temperature control platform of the IVIS machine, and imaged in vivo. After euthanization, mice were dissected and organs were imaged ex vivo. The intensity of luminescence signals was quantified by Living Image Software (PerkinElmer). This luminescence imaging method can detect as few as 50 tumor cells in the lymph node. Stereomicroscope imaging was performed with a Zeiss Axio Zoom.V16 microscope and a QImaging optiMOS sCMOS camera (QImaging), combined with a light-emitting diode illumination system (pE-4000, CoolLED Ltd.).

Cell lines

B16F10 cells expressing luciferase (luc2) and tdTomato were generated and described previously (*30*). Cells were cultured in Dulbecco's modified Eagle medium (DMEM) containing GlutaMAX, pyruvate, 10% fetal bovine serum (FBS), and penicillin/streptomycin (Gibco/Thermo Fisher). G418 (1.5 mg/ml; Roche) was added to the culture medium to ensure stable expression of the tdTomato transgene. 4T1 mammary carcinoma cells expressing luciferase (luc2) (PerkinElmer) were maintained in DMEM supplemented with L-glutamine, 10% FBS, and penicillin/streptomycin under standard culture conditions (37°C, 5% CO_2).

RNA extraction and qPCR

RNA from snap-frozen tissues was extracted using the NucleoSpin RNA Kit (Macherey-Nagel) according to the manufacturer's instructions. The intestinal tissue was snap-frozen after removal of the fat tissue, and RNA was extracted using the RNeasy Lipid Tissue Mini Kit (Qiagen). RNA was reverse-transcribed using the High-Capacity cDNA Kit (Applied Biosystems/Thermo Fisher). qPCR analyses were performed on a 7900HT FAST instrument (Applied Biosystems/Thermo Fisher) in triplicate using SYBR Green (Roche). *RPLP0* was used as an internal reference gene. Relative expression (RE) was calculated according to the formula $RE_{geneX} = 2^{-(CtgeneX - CtRPLP0)}$ and was expressed as fold change normalized to the control condition. The primer sequences used for qPCR were as follows: RPLP0, 5′-AGATTCGGGATATGCTGTTGG-3′ (forward) and 5′-TCGGGTCCTAGACCAGTGTTC-3′ (reverse); VEGFC, 5′-GGGGGCGAGGTCAAGGCTTTT-3′ (forward) and 5′-CCTGGTATTGAGGGTGGGCTGC-3′ (reverse).

Enzyme-linked immunosorbent assay

Tissue samples were resected, snap-frozen, and kept at −80°C. Blood (500 μl) was collected in Capiject tubes (Terumo), left at room temperature for 20 min, and centrifuged at 1200*g* for 10 min. The serum was collected, snap-frozen, and kept at −80°C. For each tissue sample, 100 mg of tissue was homogenized in 1 ml of PBS and diluted by 1:250 (lung and intestine) or 1:5000 (liver) with PBS before measurements. Mouse VEGF-C levels were measured using a mouse VEGF-C ELISA kit (Cusabio), following the manufacturer's instructions.

Lung homing assay

B16F10-luc2-tdTomato cells (1×10^6) were injected into the tail vein. After 24 hours, the lung was perfused, resected, minced, and digested in a collagenase solution (Collagenase II, 2 mg/ml, Sigma-Aldrich; deoxyribonuclease I, 40 μg/ml, Roche) for 45 min at 37°C. The digested tissue was passed through a 40-μm cell strainer before erythrocyte lysis with Pharm Lyse (BD). After washing and a second filtration step, the cell suspension was labeled with CD45-APC/Cy7 (103116, BioLegend). 7-AAD (7-aminoactinomycin D; 420404, BioLegend) was used for life/dead discrimination. CD45-negative, tdTomato-positive cells were counted as tumor cells homed into the lungs.

Statistical analyses

Statistical analyses were performed with GraphPad Prism 5 (GraphPad Software Inc.). Graphs represent means ± SD. Student's *t* test was used to compare two groups. One-way ANOVA was used to compare three groups. Other types of tests are indicated in the text or the figure legends. A *P* value of <0.05 was considered statistically significant (indicated by asterisks).

SUPPLEMENTARY MATERIALS

Supplementary material for this article is available at http://advances.sciencemag.org/cgi/content/full/4/8/eaat4758/DC1

Fig. S1. High-magnification images of 4T1 metastases in lung sections stained for Thy1 and cytokeratin.
Fig. S2. Clinical characteristics of study cohorts.
Fig. S3. Lymphatic density and its correlation with prognosis.
Fig. S4. Correlation of LV density and immune cell infiltration in lung metastases of melanoma patients.
Fig. S5. Quantification of the number and size distribution of lung metastatic nodules in the B16F10 model.
Fig. S6. Quantification of VEGF-C levels and analysis of LVs in different organs.
Fig. S7. Characterization of CCSP-rtTA × tet-O–VEGF-C mice on BALB/c background.
Fig. S8. Comparison of 4T1 primary tumor growth and lung metastasis without VEGF-C induction.
Fig. S9. Quantification of nodule numbers and size distribution of the lung metastases on day PR21 in the 4T1 model.
Fig. S10. 4T1 metastases in distant organs.

REFERENCES AND NOTES

1. S. A. Stacker, S. P. Williams, T. Karnezis, R. Shayan, S. B. Fox, M. G. Achen, Lymphangiogenesis and lymphatic vessel remodelling in cancer. *Nat. Rev. Cancer* **14**, 159–172 (2014).
2. S. Karaman, M. Detmar, Mechanisms of lymphatic metastasis. *J. Clin. Invest.* **124**, 922–928 (2014).
3. L. C. Dieterich, M. Detmar, Tumor lymphangiogenesis and new drug development. *Adv. Drug Deliv. Rev.* **99**, 148–160 (2016).
4. S. Hirakawa, S. Kodama, R. Kunstfeld, K. Kajiya, L. F. Brown, M. Detmar, VEGF-A induces tumor and sentinel lymph node lymphangiogenesis and promotes lymphatic metastasis. *J. Exp. Med.* **201**, 1089–1099 (2005).
5. S. Hirakawa, L. F. Brown, S. Kodama, K. Paavonen, K. Alitalo, M. Detmar, VEGF-C–induced lymphangiogenesis in sentinel lymph nodes promotes tumor metastasis to distant sites. *Blood* **109**, 1010–1017 (2007).
6. R. Liersch, S. Hirakawa, W. E. Berdel, R. M. Mesters, M. Detmar, Induced lymphatic sinus hyperplasia in sentinel lymph nodes by VEGF-C as the earliest premetastatic indicator. *Int. J. Oncol.* **41**, 2073–2078 (2012).
7. M. Kim, Y. J. Koh, K. E. Kim, B. I. Koh, D.-H. Nam, K. Alitalo, I. Kim, G. Y. Koh, CXCR4 signaling regulates metastasis of chemoresistant melanoma cells by a lymphatic metastatic niche. *Cancer Res.* **70**, 10411–10421 (2010).
8. A. W. Lund, F. V. Duraes, S. Hirosue, V. R. Raghavan, C. Nembrini, S. N. Thomas, A. Issa, S. Hugues, M. A. Swartz, VEGF-C promotes immune tolerance in B16 melanomas and cross-presentation of tumor antigen by lymph node lymphatics. *Cell Rep.* **1**, 191–199 (2012).

9. K. Naxerova, J. G. Reiter, E. Brachtel, J. K. Lennerz, M. van de Wetering, A. Rowan, T. Cai, H. Clevers, C. Swanton, M. A. Nowak, S. J. Elledge, R. K. Jain, Origins of lymphatic and distant metastases in human colorectal cancer. *Science* **357**, 55–60 (2017).
10. G. Gundem, P. van Loo, B. Kremeyer, L. B. Alexandrov, J. M. C. Tubio, E. Papaemmanuil, D. S. Brewer, H. M. L. Kallio, G. Högnäs, M. Annala, K. Kivinummi, V. Goody, C. Latimer, S. O'Meara, K. J. Dawson, W. Isaacs, M. R. Emmert-Buck, M. Nykter, C. Foster, Z. Kote-Jarai, D. Easton, H. C. Whitaker; ICGC Prostate UK Group, D. E. Neal, C. S. Cooper, R. A. Eeles, T. Visakorpi, P. J. Campbell, U. McDermott, D. C. Wedge, G. S. Bova, The evolutionary history of lethal metastatic prostate cancer. *Nature* **520**, 353–357 (2015).
11. M. K. H. Hong, G. Macintyre, D. C. Wedge, P. Van Loo, K. Patel, S. Lunke, L. B. Alexandrov, C. Sloggett, M. Cmero, F. Marass, D. Tsui, S. Mangiola, A. Lonie, H. Naeem, N. Sapre, P. M. Phal, N. Kurganovs, X. Chin, M. Kerger, A. Y. Warren, D. Neal, V. Gnanapragasam, N. Rosenfeld, J. S. Pedersen, A. Ryan, I. Haviv, A. J. Costello, N. M. Corcoran, C. M. Hovens, Tracking the origins and drivers of subclonal metastatic expansion in prostate cancer. *Nat. Commun.* **6**, 6605 (2015).
12. A. E. Giuliano, K. K. Hunt, K. V. Ballman, P. D. Beitsch, P. W. Whitworth, P. W. Blumencranz, A. M. Leitch, S. Saha, L. M. McCall, M. Morrow, Axillary dissection vs no axillary dissection in women with invasive breast cancer and sentinel node metastasis: A randomized clinical trial. *JAMA* **305**, 569–575 (2011).
13. V. Galimberti, B. F. Cole, S. Zurrida, G. Viale, A. Luini, P. Veronesi, P. Baratella, C. Chifu, M. Sargenti, M. Intra, O. Gentilini, M. G. Mastropasqua, G. Mazzarol, S. Massarut, J. R. Garbay, J. Zgajnar, H. Galatius, A. Recalcati, D. Littlejohn, M. Bamert, M. Colleoni, K. N. Price, M. M. Regan, A. Goldhirsch, A. S. Coates, R. D. Gelber, U. Veronesi; International Breast Cancer Study Group Trial 23-01 investigators, Axillary dissection versus no axillary dissection in patients with sentinel-node micrometastases (IBCSG 23-01): A phase 3 randomised controlled trial. *Lancet Oncol.* **14**, 297–305 (2013).
14. M. B. Faries, J. F. Thompson, A. J. Cochran, R. H. Andtbacka, N. Mozzillo, J. S. Zager, T. Jahkola, T. L. Bowles, A. Testori, P. D. Beitsch, H. J. Hoekstra, M. Moncrieff, C. Ingvar, M. W. J. M. Wouters, M. S. Sabel, E. A. Levine, D. Agnese, M. Henderson, R. Dummer, C. R. Rossi, R. I. Neves, S. D. Trocha, F. Wright, D. R. Byrd, M. Matter, E. Hsueh, A. MacKenzie-Ross, D. B. Johnson, P. Terheyden, A. C. Berger, T. L. Huston, J. D. Wayne, B. M. Smithers, H. B. Neuman, S. Schneebaum, J. E. Gershenwald, C. E. Ariyan, D. C. Desai, L. Jacobs, K. M. McMasters, A. Gesierich, P. Hersey, S. D. Bines, J. M. Kane, R. J. Barth, G. McKinnon, J. M. Farma, E. Schultz, S. Vidal-Sicart, R. A. Hoefer, J. M. Lewis, R. Scheri, M. C. Kelley, O. E. Nieweg, R. D. Noyes, D. S. B. Hoon, H. J. Wang, D. A. Elashoff, R. M. Elashoff, Completion dissection or observation for sentinel-node metastasis in melanoma. *N. Engl. J. Med.* **376**, 2211–2222 (2017).
15. S. Kretschmer, I. Dethlefsen, S. Hagner-Benes, L. M. Marsh, H. Garn, P. König, Visualization of intrapulmonary lymph vessels in healthy and inflamed murine lung using CD90/Thy-1 as a marker. *PLOS ONE* **8**, e55201 (2013).
16. G. Jurisic, M. Iolyeva, S. T. Proulx, C. Halin, M. Detmar, Thymus cell antigen 1 (Thy1, CD90) is expressed by lymphatic vessels and mediates cell adhesion to lymphatic endothelium. *Exp. Cell Res.* **316**, 2982–2992 (2010).
17. D. T. Mzinza, H. Fleige, K. Laarmann, S. Willenzon, J. Ristenpart, J. Spanier, G. Sutter, U. Kalinke, P. Valentin-Weigand, R. Förster, Application of light sheet microscopy for qualitative and quantitative analysis of bronchus-associated lymphoid tissue in mice. *Cell. Mol. Immunol.* (2018).
18. X. Xu, P. A. Gimotty, D. Guerry, G. Karakousis, P. Van Belle, H. Liang, K. Montone, T. Pasha, M. E. Ming, G. Acs, M. Feldman, S. Barth, R. Hammond, R. Elenitsas, P. J. Zhang, D. E. Elder, Lymphatic invasion revealed by multispectral imaging is common in primary melanomas and associates with prognosis. *Hum. Pathol.* **39**, 901–909 (2008).
19. K. Doeden, Z. Ma, B. Narasimhan, S. M. Swetter, M. Detmar, S. S. Dadras, Lymphatic invasion in cutaneous melanoma is associated with sentinel lymph node metastasis. *J. Cutan. Pathol.* **36**, 772–780 (2009).
20. Y. Ino, R. Yamazaki-Itoh, K. Shimada, M. Iwasaki, T. Kosuge, Y. Kanai, N. Hiraoka, Immune cell infiltration as an indicator of the immune microenvironment of pancreatic cancer. *Br. J. Cancer* **108**, 914–923 (2013).
21. D. S. Behr, W. K. Peitsch, C. Hametner, F. Lasitschka, R. Houben, K. Schönhaar, J. Michel, C. Dollt, M. Goebeler, A. Marx, S. Goerdt, A. Schmieder, Prognostic value of immune cell infiltration, tertiary lymphoid structures and PD-L1 expression in Merkel cell carcinomas. *Int. J. Clin. Exp. Pathol.* **7**, 7610–7621 (2014).
22. L.-C. Yao, C. Testini, D. Tvorogov, A. Anisimov, S. O. Vargas, P. Baluk, B. Pytowski, L. Claesson-Welsh, K. Alitalo, D. M. McDonald, Pulmonary lymphangiectasia resulting from vascular endothelial growth factor-C overexpression during a critical period. *Circ. Res.* **114**, 806–822 (2014).
23. P. Baluk, L.-C. Yao, J. C. Flores, D. Choi, Y.-K. Hong, D. M. McDonald, Rapamycin reversal of VEGF-C–driven lymphatic anomalies in the respiratory tract. *JCI Insight* **2**, e90103 (2017).
24. S. Das, D. S. Ladell, S. Podgrabinska, V. Ponomarev, C. Nagi, J. T. Fallon, M. Skobe, Vascular endothelial growth factor-C induces lymphangitic carcinomatosis, an extremely aggressive form of lung metastases. *Cancer Res.* **70**, 1814–1824 (2010).
25. S. T. Boyle, W. V. Ingman, V. Poltavets, J. W. Faulkner, R. J. Whitfield, S. R. McColl, M. Kochetkova, The chemokine receptor CCR7 promotes mammary tumorigenesis through amplification of stem-like cells. *Oncogene* **35**, 105–115 (2016).
26. M. Lohela, H. Heloterä, P. Haiko, D. J. Dulmont, K. Alitalo, Transgenic induction of vascular endothelial growth factor-C is strongly angiogenic in mouse embryos but leads to persistent lymphatic hyperplasia in adult tissues. *Am. J. Pathol.* **173**, 1891–1901 (2008).
27. M. Jeltsch, A. Kaipainen, V. Joukov, X. Meng, M. Lakso, H. Rauvala, M. Swartz, D. Fukumura, R. K. Jain, K. Alitalo, Hyperplasia of lymphatic vessels in VEGF-C transgenic mice. *Science* **276**, 1423–1425 (1997).
28. V. Joukov, T. Sorsa, V. Kumar, M. Jeltsch, L. Claesson-Welsh, Y. Cao, O. Saksela, N. Kalkkinen, K. Alitalo, Proteolytic processing regulates receptor specificity and activity of VEGF-C. *EMBO J.* **16**, 3898–3911 (1997).
29. I. Choi, H. K. Chung, S. Ramu, H. N. Lee, K. E. Kim, S. Lee, J. Yoo, D. Choi, Y. S. Lee, B. Aguilar, Y.-K. Hong, Visualization of lymphatic vessels by *Prox1*-promoter directed GFP reporter in a bacterial artificial chromosome-based transgenic mouse. *Blood* **117**, 362–365 (2011).
30. S. T. Proulx, P. Luciani, A. Christiansen, S. Karaman, K. S. Blum, M. Rinderknecht, J.-C. Leroux, M. Detmar, Use of a PEG-conjugated bright near-infrared dye for functional imaging of rerouting of tumor lymphatic drainage after sentinel lymph node metastasis. *Biomaterials* **34**, 5128–5137 (2013).

Acknowledgments: We thank K. Alitalo for providing tet-O–VEGF-C mice; J. Scholl, J. Forrer, C. Ochoa, the Rodent Center HCI team, and the Scientific Center for Optical and Electron Microscopy (ScopeM) for excellent technical assistance; and A. Steingötter (Statistical Consulting Group, Seminar for Statistics, ETH Zurich) for the support in statistical analysis. **Funding:** This work was supported by the Swiss National Science Foundation (grants 3100A0-108207 and 31003A-130627 to M.D.), the European Research Council (Advanced grant LYVICAM to M.D.), the Leducq Transatlantic Network of Excellence on Lymph Vessels in Obesity and Cardiovascular Disease (grant 11CVD03 to M.D. and D.M.M.), and the U.S. NIH National Heart, Lung, and Blood Institute (grants R01 HL059157, R01 HL127402, and P01 HL024136 to D.M.M.). **Author contributions:** Q.M. conceived and designed the study, performed the experiments, analyzed and interpreted data, and drafted the manuscript. L.C.D. conceived and designed the study, discussed the experiments, interpreted data, and drafted the manuscript. K.I., J.M., and V.C.A. analyzed data of the retrospective study. M.P.L. and R.D. conceived and designed the retrospective study and discussed the experiments. S.B.B. performed the experiments and acquired data. S.T.P. performed the stereomicroscope imaging, discussed the experiments, and edited the manuscript. P.B. and D.M.M. bred CCSP-rtTA × tet-O–VEGF-C mice, discussed the experiments, and edited the manuscript. M.D. conceived and designed the study, interpreted data, supervised the progress, and drafted the manuscript. All authors have approved the final version of the manuscript and have agreed to be accountable for all aspects of the work. **Competing interests:** The authors declare that they have no competing interests. **Data and materials availability:** All data needed to evaluate the conclusions in the paper are present in the paper and/or the Supplementary Materials. Additional data related to this paper may be requested from the authors.

Submitted 13 March 2018
Accepted 26 June 2018
Published 8 August 2018
10.1126/sciadv.aat4758

Citation: Q. Ma, L. C. Dieterich, K. Ikenberg, S. B. Bachmann, J. Mangana, S. T. Proulx, V. C. Amann, M. P. Levesque, R. Dummer, P. Baluk, D. M. McDonald, M. Detmar, Unexpected contribution of lymphatic vessels to promotion of distant metastatic tumor spread. *Sci. Adv.* **4**, eaat4758 (2018).